Atmospheric Chemistry of $CF_3CH_2OCH_2CF_3$: UV Spectra and Kinetic Data for $CF_3CH(\bullet)OCH_2CF_3$ and $CF_3CH(OO\bullet)OCH_2CF_3$ Radicals and Atmospheric Fate of $CF_3CH(O\bullet)OCH_2CF_3$ Radicals

T. J. Wallington* and A. Guschin

Ford Research Laboratory, SRL-3083, Ford Motor Company, P.O. Box 2053, Dearborn, Michigan 48121-2053

T. N. N. Stein, J. Platz, J. Sehested, L. K. Christensen, and O. J. Nielsen

Atmospheric Chemistry, Building 313, Plant Biology and Biogeochemistry Department, Risø National Laboratory, DK-4000 Roskilde, Denmark

Received: September 8, 1997; In Final Form: December 1, 1997

Pulse radiolysis transient UV absorption spectroscopy was used to study the ultraviolet absorption spectra (220−320 nm) and kinetics of $CF_3CH(\bullet)OCH_2CF_3$ and $CF_3CH(OO\bullet)OCH_2CF_3$ radicals at 296 K. At 230 nm $\sigma(CF_3CH(\bullet)OCH_2CF_3) = (1.95 \pm 0.24) \times 10^{-18}$ and $\sigma(CF_3CH(OO\bullet)OCH_2CF_3) = (4.40 \pm 0.51) \times 10^{-18}$ cm^2 molecule^{-1}. Rate constants for the reaction of F atoms with $CF_3CH_2OCH_2CF_3$, the self-reactions of $CF_3CH(\bullet)OCH_2CF_3$ and $CF_3CH(OO\bullet)OCH_2CF_3$ radicals, the association reaction of $CF_3CH(\bullet)OCH_2CF_3$ radicals with O_2, and the reactions of $CF_3CH(OO\bullet)OCH_2CF_3$ radicals with NO and NO_2 were $(1.5 \pm 0.7) \times 10^{-11}$, $(2.6 \pm 0.4) \times 10^{-11}$, $(5.4 \pm 0.7) \times 10^{-12}$ (uncorrected for possible secondary chemistry), $(2.3 \pm 0.3) \times 10^{-12}$, $(1.45 \pm 0.4) \times 10^{-11}$, and $(8.4 \pm 0.8) \times 10^{-12}$ cm^3 molecule^{-1} s^{-1}, respectively. Using an FTIR technique, rate constants for the reaction of Cl atoms with $CF_3CH_2OCH_2CF_3$ and $CF_3C(O)OCH_2CF_3$ were determined to be $(7.1 \pm 0.9) \times 10^{-13}$ and $(9.4 \pm 1.3) \times 10^{-16}$ cm^3 molecule^{-1} s^{-1}. Finally, it was determined that the atmospheric fate of $CF_3CH(O\bullet)OCH_2CF_3$ radicals is decomposition via C−C bond scission to give CF_3 radicals and 2,2,2-trifluoroethyl formate (CF_3CH_2OCHO) which occurs at a rate of approximately 7×10^5 s^{-1}. The results are discussed with respect to the atmospheric chemistry of $CF_3CH_2OCH_2CF_3$ and analogous compounds.

1. Introduction

Recognition of the adverse effect of chlorofluorocarbon (CFC) release into the atmosphere[1,2] has led to an international effort to replace CFCs with environmentally acceptable alternatives. Hydrofluoroethers (HFEs) are fluid compounds which have been developed to replace CFCs in applications such as the cleaning of electronic equipment, heat-transfer agents in refrigeration systems, and carrier fluids for lubricant deposition. Bis(2,2,2-trifluoroethyl) ether ($CF_3CH_2OCH_2CF_3$) is a volatile liquid with a boiling point of 62−63 °C and a vapor pressure of 115 Torr at 19 °C. We are interested in this compound because it may find application as a CFC replacement and because a study of its atmospheric chemistry sheds light on the environmental impact of commercial HFEs such as $C_4F_9OCH_3$ (HFE-7100) and $C_4F_9OC_2H_5$ (HFE-7200).

The atmospheric oxidation of $CF_3CH_2OCH_2CF_3$ will be initiated by reaction with OH radicals. The alkyl radical produced in reaction 1 will add O_2 rapidly to give a peroxy radical.

$$CF_3CH_2OCH_2CF_3 + OH \rightarrow CF_3CH(\bullet)OCH_2CF_3 + H_2O \quad (1)$$

$$CF_3CH(\bullet)OCH_2CF_3 + O_2 + M \rightarrow CF_3CH(OO\bullet)OCH_2CF_3 + M \quad (2)$$

By analogy to other peroxy radicals,[3] $CF_3CH(OO\bullet)OCH_2CF_3$ radicals will react with NO, NO_2, HO_2, and other peroxy radicals in the atmosphere.

$$CF_3CH(OO\bullet)OCH_2CF_3 + NO \rightarrow CF_3CH(O\bullet)OCH_2CF_3 + NO_2 \quad (3a)$$

$$CF_3CH(OO\bullet)OCH_2CF_3 + NO + M \rightarrow CF_3CH(ONO_2)OCH_2CF_3 + M \quad (3b)$$

$$CF_3CH(OO\bullet)OCH_2CF_3 + NO_2 + M \rightarrow CF_3CH(OONO_2)OCH_2CF_3 + M \quad (4)$$

$$CF_3CH(OO\bullet)OCH_2CF_3 + HO_2 \rightarrow \text{products} \quad (5)$$

$$CF_3CH(OO\bullet)OCH_2CF_3 + R'O_2 \rightarrow \text{products} \quad (6)$$

Experiments have been performed in our laboratories to elucidate the atmospheric chemistry of $CF_3CH_2OCH_2CF_3$. A pulse radiolysis time-resolved UV−visible spectroscopic technique was used at Risø to measure the UV absorption spectra of $CF_3CH(\bullet)OCH_2CF_3$ and $CF_3CH(OO\bullet)OCH_2CF_3$ radicals and to study the kinetics of reactions 2, 3, 4, and 6. In the case of reaction 6 we studied the self-reaction of the peroxy radical ($R'O_2 = CF_3CH(OO\bullet)OCH_2CF_3$). The fate of the alkoxy radical $CF_3CH(O\bullet)OCH_2CF_3$ produced in reaction 3a was determined using a FTIR spectrometer coupled to a smog chamber at Ford Motor Company. The results are reported herein and discussed

S1089-5639(97)02933-2 CCC: $15.00
Published on Web 01/27/1998

with respect to the environmental impact of bis(2,2,2-trifluoroethyl) ether and other HFEs.

2. Experimental Section

The two experimental systems used are described in detail elsewhere.[4−6]

2.1. Pulse Radiolysis System at Risø National Laboratory. A pulse radiolysis transient UV absorption apparatus[4] was used to study the UV absorption spectra and kinetics of $CF_3CH(\bullet)OCH_2CF_3$ and $CF_3CH(OO\bullet)OCH_2CF_3$ radicals. Radicals were generated by radiolysis of gas mixtures in a 1 L stainless steel reactor by a 30 ns pulse of 2 MeV electrons from a Febetron 705B field emission accelerator. The radiolysis dose, referred to herein as a fraction of maximum dose, was varied by insertion of stainless steel attenuators between the accelerator and the chemical reactor. The analyzing light was provided by a pulsed Xenon arc lamp, reflected in the reaction cell by internal White type optics, dispersed using a 1 m McPherson monochromator (operated at a spectral resolution of 0.8 nm), and detected by a photomultiplier. All transients were results of single-pulse experiments with no signal averaging.

SF_6 was used as the diluent gas. Radiolysis of SF_6 produces fluorine atoms:

$$SF_6 + 2\ \text{MeV}\ e^- \rightarrow F + \text{products} \qquad (7)$$

SF_6 was always present in great excess to minimize the relative importance of direct radiolysis of other compounds in the gas mixtures. The fluorine atom yield was determined by measuring the yield of CH_3O_2 radicals following radiolysis of mixtures of 10 mbar CH_4, 40 mbar O_2, and 950 mbar SF_6:

$$F + CH_4 \rightarrow CH_3 + HF \qquad (8)$$

$$CH_3 + O_2 + M \rightarrow CH_3O_2 + M \qquad (9)$$

CH_3O_2 radicals were monitored using their absorption at 260 nm. On the basis of $\sigma_{260\ nm}(CH_3O_2) = 3.18 \times 10^{-18}$ cm^2 molecule^{-1} [7] the F atom yield at full radiolysis dose and 1000 mbar SF_6 was determined to be $(2.98 \pm 0.33) \times 10^{15}$ cm^{-3} (760 Torr = 1013 mbar). The quoted uncertainty reflects both statistical uncertainties associated with the calibration procedure and a 10% uncertainty in $\sigma(CH_3O_2)$.[7]

Reagents used were the following: 0−30 mbar O_2 (ultrahigh purity), 950−1000 mbar SF_6 (99.9%), 0−31.1 mbar $CF_3CH_2OCH_2CF_3$ (>99%), 0−1.02 mbar NO (>99.8%), 0−0.69 mbar NO_2 (>98%), and 0−50 mbar of CF_3CCl_2H (>99%). All were used as received. The $CF_3CH_2OCH_2CF_3$ sample was repeatedly degassed by freeze−pump−thaw cycles before use. Four sets of experiments were performed using the pulse radiolysis system. First, the radiolysis of $SF_6/CF_3CH_2OCH_2CF_3$ mixtures was used to study the UV spectrum and kinetics of the $CF_3CH(\bullet)OCH_2CF_3$ alkyl radical. Second, the radiolysis of $SF_6/CF_3CH_2OCH_2CF_3/CF_3CCl_2H$ mixtures was employed to study the competition for F atoms by $CF_3CH_2OCH_2CF_3$ and CF_3CCl_2H and thereby to measure the rate of reaction of F atoms with $CF_3CH_2OCH_2CF_3$. Third, the radiolysis of $SF_6/CF_3CH_2OCH_2CF_3/O_2$ mixtures was used to study the UV spectrum and kinetics of the $CF_3CH(OO\bullet)OCH_2CF_3$ alkyl peroxy radical. Finally, the radiolysis of $SF_6/CF_3CH_2OCH_2CF_3/O_2/NO_x$ mixtures was used to study the rates of reaction of the $CF_3CH(OO\bullet)OCH_2CF_3$ radical with NO and NO_2.

2.2. FTIR−Smog Chamber System at Ford Motor Company. All experiments were performed in a 140 L Pyrex reactor interfaced to a Mattson Sirus 100 FTIR spectrometer.[6] The reactor was surrounded by 22 fluorescent blacklamps (GE F15T8-BL). The oxidation of $CF_3CH_2OCH_2CF_3$ was initiated by reaction with Cl atoms generated by the photolysis of molecular chlorine in 700 Torr total pressure of O_2/N_2 diluent at 295 ± 2 K:

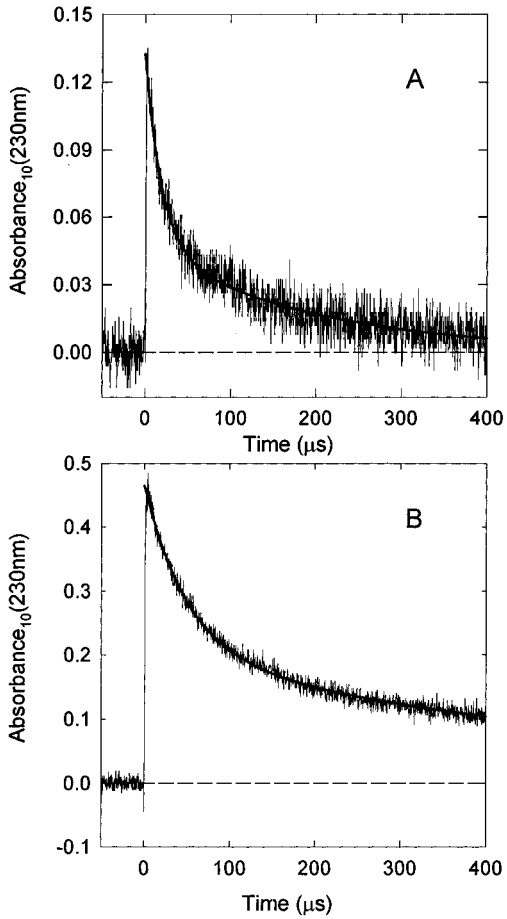

Figure 1. Transient absorptions at 230 nm following radiolysis of mixtures of (A) 10 mbar $CF_3CH_2OCH_2CF_3$ and 990 mbar SF_6 (0.32 dose) and (B) 10 mbar $CF_3CH_2OCH_2CF_3$, 30 mbar of O_2, and 960 mbar of SF_6 (0.53 dose). The UV analysis path length was 160 cm. Absorption is ascribed to (A) $CF_3CH(\bullet)OCH_2CF_3$ radicals and (B) $CF_3CH(OO\bullet)OCH_2CF_3$ radicals. The smooth lines are second-order decay fits.

$$Cl_2 + h\nu \rightarrow 2Cl \qquad (10)$$

$$Cl + CF_3CH_2OCH_2CF_3 \rightarrow CF_3CH(\bullet)OCH_2CF_3 + HCl \qquad (11)$$

$$CF_3CH(\bullet)OCH_2CF_3 + O_2 + M \rightarrow CF_3CH(OO\bullet)OCH_2CF_3 + M \qquad (2)$$

Loss of $CF_3CH_2OCH_2CF_3$ and product formation were monitored by Fourier transform infrared (FTIR) spectroscopy using an infrared path length of 28 m and a resolution of 0.25 cm^{-1}. Infrared spectra were derived from 32 co-added interferograms (the data acquisition took 1.5 min).

Radicals were generated by the UV irradiation of mixtures of 4.4−5.2 mTorr of $CF_3CH_2OCH_2CF_3$ (>99%) or 4.0−4.4 mTorr of $CF_3C(O)OCH_2CF_3$ (>99%), 90−370 mTorr of Cl_2 (research grade), 0−600 Torr of O_2 (ultrahigh purity), and 0−11 mTorr of NO (>99%) in 700 Torr of total pressure with

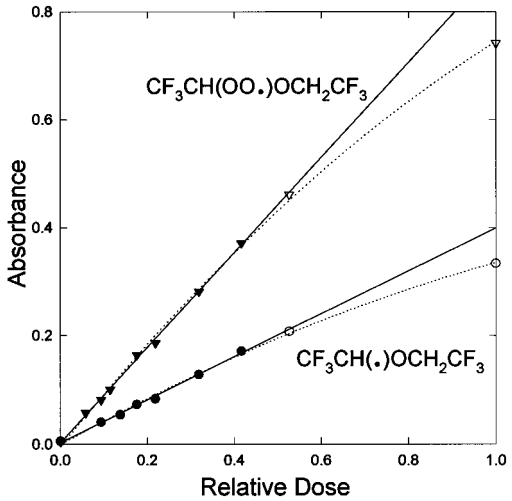

Figure 2. Maximum transient absorptions (UV path length = 160 cm) at 230 nm observed following radiolysis of mixtures of 10 mbar $CF_3CH_2OCH_2CF_3$ and 990 mbar SF_6 (circles) and 10 mbar $CF_3CH_2OCH_2CF_3$, 30 mbar of O_2, and 960 mbar of SF_6 (triangles). Solid lines are linear least-squares fits to the low-dose data (filled symbols). Dotted lines are polynomial fits to aid visual inspection of the data trend.

ultrahigh purity N_2 diluent (760 Torr = 1013 mbar). $CF_3CH_2OCH_2CF_3$, $CF_3C(O)OCH_2CF_3$, and COF_2 were monitored using their characteristic features over the wavenumber ranges 900−1400, 1780−1850, and 1880−1980 cm^{-1}, respectively. Reference spectra were acquired by expanding known volumes of reference materials into the chamber. At 1944 cm^{-1} $\sigma(COF_2) = 1.21 \times 10^{-18}$ cm^2 $molecule^{-1}$, while at 1817 cm^{-1} $\sigma(CF_3C(O)OCH_2CF_3) = 1.11 \times 10^{-18}$ cm^2 $molecule^{-1}$. Two sets of experiments were performed. First, relative rate techniques were used to determine the rate constants for reactions of Cl atoms with $CF_3CH_2OCH_2CF_3$ and $CF_3C(O)OCH_2CF_3$. Second, the products of the atmospheric oxidation of $CF_3CH_2OCH_2CF_3$ were investigated by irradiating $CF_3CH_2OCH_2CF_3/Cl_2/NO/O_2/N_2$ mixtures.

3. Results and Discussion

3.1. UV Absorption Spectrum of the $CF_3CH(\bullet)OCH_2CF_3$ Radical. Following the pulse radiolysis of mixtures of 10 mbar of $CF_3CH_2OCH_2CF_3$ and 990 mbar of SF_6, a rapid increase (complete within 1−2 μs) in absorption at 230 nm was observed, followed by a slower decay. Figure 1A shows a typical absorption transient. No absorption was observed when either 10 mbar of $CF_3CH_2OCH_2CF_3$ or 990 mbar of SF_6 was subject to pulse radiolysis separately. We ascribe the absorption in Figure 1A to formation of $CF_3CH(\bullet)OCH_2CF_3$ radicals via reaction 12 and their subsequent loss via self-reaction (13).

$$F + CF_3CH_2OCH_2CF_3 \rightarrow CF_3CH(\bullet)OCH_2CF_3 + HF \quad (12)$$

In this work we assume that F atoms react with $CF_3CH_2OCH_2CF_3$ exclusively via H atom abstraction. To determine the absorption cross section of the $CF_3CH(\bullet)OCH_2CF_3$ radical at 230 nm, the maximum transient absorbance was recorded at various radiolysis doses. Figure 2 (circles) shows a plot of the observed maximum absorbance versus the radiolysis dose (and hence initial radical concentration). The absorbance increases linearly up to 42% of full dose, suggesting that unwanted radical−radical reactions such as reactions 13 and 14, are unimportant in this range.

TABLE 1: Selected UV Absorption Cross Sections

wavelength (nm)	$\sigma(CF_3CH(\bullet)OCH_2CF_3)$ $\times 10^{20}$ (cm^2 $molecule^{-1}$)	$\sigma(CF_3CH(OO\bullet)OCH_2CF_3)$ $\times 10^{20}$ (cm^2 $molecule^{-1}$)
220	244	428
225	218	439
230	195	440
235	171	401
240	149	350
245	123	304
250	99	248
255	74	205
260	54	153
270	24	86
280	14	42
290	4	21
300	8	11
320	4	5

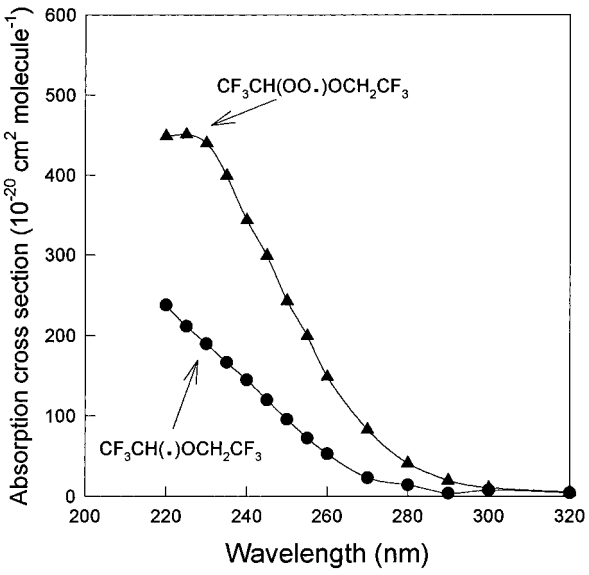

Figure 3. Spectra of the radical species $CF_3CH(\bullet)OCH_2CF_3$ (circles) and $CF_3CH(OO\bullet)OCH_2CF_3$ (triangles).

$$CF_3CH(\bullet)OCH_2CF_3 + CF_3CH(\bullet)OCH_2CF_3 + M \rightarrow \text{products} \quad (13)$$

$$F + CF_3CH(\bullet)OCH_2CF_3 \rightarrow \text{products} \quad (14)$$

Linear least squares regression of the low-dose data in Figure 2 gives a slope of 0.40 ± 0.02. Combining this result with the calibrated fluorine atom yield of (2.98 ± 0.33) × 10^{15} cm^{-3} at full dose and 1000 mbar of SF_6, and the optical path length of 160 cm gives $\sigma_{230\ nm}(CF_3CH(\bullet)OCH_2CF_3) = (1.95 \pm 0.24) \times 10^{-18}$ cm^2 $molecule^{-1}$. The UV absorption spectrum in the range 220−320 nm was mapped out by comparing the absorption at a given wavelength to that at 230 nm and scaling to $\sigma_{230\ nm} = 1.95 \times 10^{-18}$ cm^2 $molecule^{-1}$. The results are listed in Table 1 and plotted in Figure 3.

3.2. Kinetics of the Self-Reaction of $CF_3CH(\bullet)OCH_2CF_3$ Radicals. The rate constant for the self-reaction of $CF_3CH(\bullet)OCH_2CF_3$ radicals was determined by monitoring the rate of decay of the absorption at 230 nm following pulse radiolysis of mixtures of 10 mbar of $CF_3CH_2OCH_2CF_3$ and 990 mbar of SF_6. The radiolysis dose was varied between full dose and 22% of full dose. The half-lives of the decays were derived from fits to the experimental transients using a second-order expression: $A(t) = A_{inf} + (A_0 - A_{inf})/(1 + k'(A_0 - A_{inf})t)$, where $A(t)$

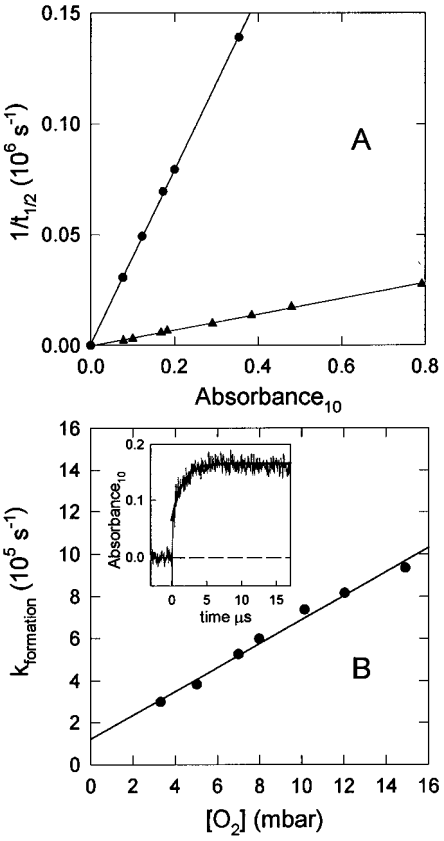

Figure 4. (A) Reciprocal half-lives for the self-reaction of $CF_3CH(\bullet)OCH_2CF_3$ (circles) and $CF_3CH(OO\bullet)OCH_2CF_3$ (triangles) radicals versus the maximum transient absorbance at 230 nm. (B) Pseudo-first-order formation rate constant of $CF_3CH(OO\bullet)OCH_2CF_3$ radicals versus the initial oxygen pressure. The inset shows a typical experimental transient (see text for details).

is the time-dependent absorbance, A_0 and A_{inf} (always close to zero) are the absorbances at $t = 0$, and at $t = \infty$, respectively, and $k' = 2k_{13}\,\sigma_{230\ nm}(CF_3CH(\bullet)OCH_2CF_3)l/\ln 10$. k_{13} is the rate constant for reaction 13 and l is the optical path length, 160 cm. The decays were always well described by the second-order expression above. An example of a fit is shown in Figure 1A. The filled circles in Figure 4A show the reciprocal of the decay half-lives at various doses versus the maximum transient absorbance. A linear regression analysis gives a slope of (3.9 ± 0.3) × 10^5 s^{-1}. This slope equals $k_{13}(2 \times 2.303)/(l\,\sigma_{230\ nm}(CF_3CH(\bullet)OCH_2CF_3))$. Hence, $k_{13} = (2.6 \pm 0.4) \times 10^{-11}$ cm^3 $molecule^{-1}$ s^{-1}. The quoted uncertainty includes uncertainties in both the slope of the line in Figure 4A and in $\sigma_{230\ nm}(CF_3CH(\bullet)OCH_2CF_3)$.

3.3. Kinetics of the F + $CF_3CH_2OCH_2CF_3$ Reaction. The rate constant ratio k_{12}/k_{15} was determined from the maximum transient absorption at 230 nm following pulse radiolysis of mixtures of 0−31.1 mbar of $CF_3CH_2OCH_2CF_3$, 50 mbar of CF_3CCl_2H, and 1000 mbar SF_6. Reactions 12 and 15 compete for the available F atoms.

$$F + CF_3CH_2OCH_2CF_3 \rightarrow CF_3CH(\bullet)OCH_2CF_3 + HF \quad (12)$$

$$F + CF_3CCl_2H \rightarrow CF_3CCl_2 + HF \quad (15)$$

The alkyl radical, CF_3CCl_2, formed by reaction of F atoms with CF_3CCl_2H (HCFC-123) absorbs strongly at 230 nm ($\sigma_{CF3CCl2}$ = 9.7 × 10^{-18} cm^2 $molecule^{-1}$ [8]). In contrast, absorption by the $CF_3CH(\bullet)OCH_2CF_3$ radical is significantly weaker ($\sigma = 1.95 \times 10^{-18}$ cm^2 $molecule^{-1}$, see section 3.1). Figure 5 shows the

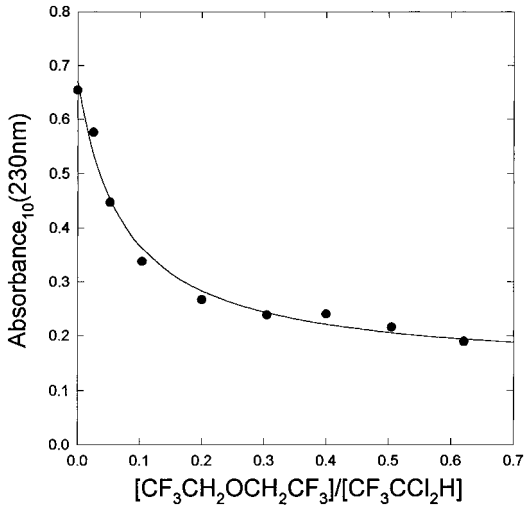

Figure 5. The maximum transient absorbance at 230 nm versus [$CF_3CH_2OCH_2CF_3$]/[CF_3CCl_2H]. The smooth line is a fit to the data; see text for details.

observed variation of the maximum transient absorbance at 230 nm as a function of the concentration ratio [$CF_3CH_2OCH_2CF_3$]/[CF_3CCl_2H] (the radiolysis dose was 0.32). The maximum transient absorption decreases with increasing $CF_3CH_2OCH_2CF_3$ concentration because a greater fraction of the F atoms react with $CF_3CH_2OCH_2CF_3$.

The data in Figure 5 can be fitted with a three-parameter expression

$$A_{max} = \frac{A_{CF3Cl2} + A_{CF3CH(\bullet)OCH2CF3}\left[\frac{k_{12}}{k_{15}}\right]\left\{\frac{[CF_3CH_2OCH_2CF_3]}{[CF_3CCl_2H]}\right\}}{1 + \left[\frac{k_{12}}{k_{15}}\right]\left\{\frac{[CF_3CH_2OCH_2CF_3]}{[CF_3CCl_2H]}\right\}}$$

where A_{max}, $A_{CF3CCl2}$, and $A_{CF3CH(\bullet)OCH2CF3}$ are the observed maximum absorbance for the mixture of radicals, the maximum absorbance expected if 100% of the F atoms were to react with CF_3CCl_2H, and the maximum absorbance expected if 100% of the F atoms were to react with $CF_3CH_2OCH_2CF_3$, respectively. $A_{CF3CCl2}$, $A_{CF3CH(\bullet)OCH2CF3}$, and k_{12}/k_{15} were simultaneously varied and the best fit was achieved with $A_{CF3CCl2} = 0.67 \pm 0.04$, $A_{CF3CH(\bullet)OCH2CF3} = 0.13 \pm 0.03$, and $k_{12}/k_{15} = 12.4 \pm 3.8$. The results for $A_{CF3CCl2}$ and $A_{C4F9OCH2}$ are consistent with those expected based on the absorption cross sections of the CF_3CCl_2 and $CF_3CH(\bullet)OCH_2CF_3$ radicals given above. Using $k_{15} = (1.2 \pm 0.4) \times 10^{-12}$ cm^3 $molecule^{-1}$ s^{-1} [9] gives $k_{12} = (1.5 \pm 0.7) \times 10^{-11}$ cm^3 $molecule^{-1}$ s^{-1}.

3.4. UV Absorption Spectrum of the $CF_3CH(OO\bullet)OCH_2CF_3$ Radical. To study the UV spectrum of the peroxy radical $CF_3CH(OO\bullet)OCH_2CF_3$, mixtures of 10 mbar of $CF_3CH_2OCH_2CF_3$, 30 mbar of O_2, and 960 mbar SF_6 were subject to pulse radiolysis, and the resulting transient absorbance was monitored at 230 nm. A typical experimental absorption is shown in Figure 1B. The maximum absorption observed at 230 nm following the radiolysis of $SF_6/CF_3CH_2OCH_2CF_3/O_2$ mixtures was approximately 2 times that observed following radiolysis of $SF_6/CF_3CH_2OCH_2CF_3$ mixtures. We attribute the absorption observed using $SF_6/CF_3CH_2OCH_2CF_3/O_2$ mixtures to the formation of $CF_3CH(OO\bullet)OCH_2CF_3$ radicals via reactions 12 and 2.

To derive the UV absorption spectrum of the $CF_3CH(OO\bullet)OCH_2CF_3$ radical we need to work under conditions where

unwanted secondary radical−radical reactions such as reactions 13, 14, and 16−18 are avoided or minimized.

$$CF_3CH(OO\bullet)OCH_2CF_3 + CF_3CH(OO\bullet)OCH_2CF_3 \rightarrow \text{products} \quad (16)$$

$$CF_3CH(OO\bullet)OCH_2CF_3 + CF_3CH(\bullet)OCH_2CF_3 \rightarrow \text{products} \quad (17)$$

$$CF_3CH(OO\bullet)OCH_2CF_3 + F \rightarrow \text{products} \quad (18)$$

In addition, the reaction of F atoms with O_2 needs to be minimized:

$$F + O_2 + M \rightarrow FO_2 + M \quad (19)$$

To minimize the amount of F atoms consumed by reaction 19, the oxygen concentration should be low. However, a low oxygen concentration will increase the importance of reactions 13, 14, and 17. Clearly, a compromise is needed. An initial O_2 concentration of 30 mbar was chosen. Under these experimental conditions 3.7% of the F atoms are converted into FO_2 ($k_{19} = 1.9 \times 10^{-13}$ [10] and $k_{12} = 1.5 \times 10^{-11}$ cm^3 molecule^{-1} s^{-1}). Absolute values for the absorption cross sections (in units of 10^{-20} cm^2 molecule^{-1}) of FO_2 at different wavelengths are[10] $\sigma_{225\ nm} = 755$, $\sigma_{230\ nm} = 508$, $\sigma_{235\ nm} = 341$, $\sigma_{240\ nm} = 180$, $\sigma_{245\ nm} = 153$, and $\sigma_{254\ nm} = 69$ and can be used to correct for the absorbance caused by FO_2 radicals.

There are no literature data concerning the kinetics of reactions 14, 17, and 18, so we cannot calculate their importance. To check for these unwanted radical−radical reactions the transient absorption at 230 nm was measured in experiments using $[CF_3CH_2OCH_2CF_3] = 10$ mbar, $[O_2] = 30$ mbar, and $[SF_6] = 960$ mbar with the radiolysis dose (and hence initial radical concentration) varied over 1 order of magnitude. The UV path length was 160 cm. The triangles in Figure 2 show the observed maximum transient absorption as a function of the dose. As seen from Figure 2, the absorption is linear with radiolysis dose up to 42% of maximum dose. This linearity indicates that at low radiolysis doses unwanted secondary radical−radical reactions are not important. The solid line drawn through the data in Figure 2 is a linear least-squares fit to the low-dose data which gives a slope of 0.88 ± 0.03. From this and three additional pieces of information, (i) the F atom yield of $(2.98 \pm 0.33) \times 10^{15}$ cm^{-3} (full dose and $[SF_6] = 1000$ mbar), (ii) the conversion of F atoms into $CF_3CH(OO\bullet)OCH_2CF_3$ (96.3%) and FO_2 (3.7%), and (iii) the absorption cross section for FO_2 at 230 nm ($\sigma = 5.08 \times 10^{-18}$ cm^2 molecule^{-1} [10]), we derive $\sigma(CF_3CH(OO\bullet)OCH_2CF_3)$ at 230 nm $= (4.40 \pm 0.51) \times 10^{-18}$ cm^2 molecule^{-1}. The quoted uncertainty reflects two standard deviations from a linear least-squares fit to the low-dose data in Figure 2 and uncertainty in the absolute calibration of the fluorine atom yield.

To map out the spectrum of the $CF_3CH(OO\bullet)OCH_2CF_3$ radical, the maximum transient absorbance was measured over the range 220−320 nm, scaled to that at 230 nm, and placed on an absolute basis using $\sigma(230\ nm) = 4.40 \times 10^{-18}$ cm^2 molecule^{-1}. Corrections were applied to account for the formation of FO_2 using the formula $\sigma_{corrected} = (\sigma_{raw} - \sigma_{FO2})0.037)/0.963$ where σ_{raw} is the cross section calculated assuming 100% yield of RO_2 radicals. The results are plotted in Figure 3 and listed in Table 1. The UV spectra of alkyl peroxy radicals typically consist of a single broad structureless feature in the region 200−300 nm with a width of 40−50 nm and a maximum cross section located at 235−245 nm of (4−5) $\times 10^{-18}$ cm^2 molecule^{-1}.[7,11] Fluorine substitution results in a blue shift of 10−20 nm.[7,11] The spectrum for the $CF_3CH(OO\bullet)OCH_2CF_3$ radical shown in Figure 3 is consistent with that expected based upon the published spectra of other peroxy radicals.

3.5. Association Reaction between O_2 and the $CF_3CH(\bullet)OCH_2CF_3$ Radical. The rate constant for the reaction between $CF_3CH(\bullet)OCH_2CF_3$ radicals and O_2 was measured by monitoring the rate of increase in absorption at 230 nm at short times (1−10 μs) following pulsed radiolysis (35−42% dose) of mixtures of 10 mbar of $CF_3CH_2OCH_2CF_3$, 3.3−14.9 mbar of O_2, and 990 mbar of SF_6. The inset in Figure 4B shows the transient recorded using 7.98 mbar of O_2. As discussed above, the peroxy radical $CF_3CH(OO\bullet)OCH_2CF_3$ absorbs strongly at 230 nm ($\sigma = 4.4 \times 10^{-18}$ cm^2 molecule^{-1}) and its formation can be monitored easily. In the presence of 10 mbar of $CF_3CH_2OCH_2CF_3$ the lifetime of F atoms with respect to conversion into alkyl radicals is 0.27 μs. At 1 μs after the radiolysis pulse the conversion of F atoms into $CF_3CH(\bullet)OCH_2CF_3$ radicals is 97% complete. The observed increase in absorption at times greater than 1 μs (see inset in Figure 4B) followed first-order kinetics and increased with increasing O_2 partial pressure. We ascribe this increase in absorption to the formation of $CF_3CH(OO\bullet)OCH_2CF_3$ radicals via reaction 2. A first-order rise expression was fit to the increase in absorption at reaction times of 1−10 μs. The expression used was $A(t) = (A_0 - A_{inf})\exp(-k_{formation}t) + A_{inf}$, where $k_{formation}$ is the pseudo-first-order formation rate constant, $A(t)$ is the absorbance as a function of time, A_0 is the maximum absorbance by $CF_3CH(\bullet)OCH_2CF_3$ radicals, and A_{inf}, is the maximum absorbance by $CF_3CH(OO\bullet)OCH_2CF_3$ radicals. $k_{formation}$, A_0, and A_{inf} were used as fit parameters. The pseudo-first-order formation rate constants ($k_{formation}$) are plotted as function of $[O_2]$ in Figure 4B. Linear least-squares analysis gives $k_2 = (2.3 \pm 0.3) \times 10^{-12}$ cm^3 molecule^{-1} s^{-1}. The y-axis intercept in Figure 4B is $(1.2 \pm 0.6) \times 10^5$ s^{-1}, which we attribute to the influence of loss of $CF_3CH(\bullet)OCH_2CF_3$ and $CF_3CH(OO\bullet)OCH_2CF_3$ radicals via their self-reactions. The measured value of k_2 is typical for addition of O_2 to an alkyl radical, which typically lie in the range $(1-5) \times 10^{-12}$ cm^3 molecule^{-1} s^{-1}.[7,11]

3.6. Kinetics of the Self-Reaction of $CF_3CH(OO\bullet)OCH_2CF_3$ Radicals. Figure 1B shows a typical transient absorption observed following the pulsed radiolysis of $CF_3CH_2OCH_2CF_3/SF_6/O_2$ mixtures. The decay of the absorption is due to the self-reaction of the $CF_3CH(OO\bullet)OCH_2CF_3$ radical:

$$CF_3CH(OO\bullet)OCH_2CF_3 + CF_3CH(OO\bullet)OCH_2CF_3 \rightarrow \text{products} \quad (16)$$

The rate constant of reaction 16 is defined by the equation $-d[RO_2]/dt = 2k_{16obs}[RO_2]^2$. The observed rate constant k_{16obs} for reaction 16 can be obtained from a plot of the reciprocal half-lives of the peroxy radical decay versus the maximum transient absorbance measured at 230 nm. The triangles in Figure 4A show such a plot. The absorbances have been corrected for the absorption due to FO_2 according to the formula $A = A_{obs} - \sigma(FO_2) \times 160$ cm $\times 0.037 \times 2.98 \times 10^{15}$ molecule cm^{-3} $\times$ dose. The decay half-lives were derived from a fit to the transients using the second-order expression $A(t) = A_{inf} + (A_0 - A_{inf})/(1 + k'(A_0 - A_{inf})t)$, where $A(t)$ is the time-dependent absorbance, A_0 and A_{inf} are the absorbances at $t = 0$, and at $t = \infty$, respectively. $k' = 2k_{16obs} \ln 10/(l\ \sigma_{RO2}(230\ nm))$ where k_{16obs} is the observed second-order rate constant for the self-reaction

of the radicals. The decays were always well described by second-order kinetics. For these experiments the optical path length (l) was 160 cm, $[CF_3CH_2OCH_2CF_3] = 10$ mbar, $[O_2] = 30$ mbar, $[SF_6] = 960$ mbar, and the dose was varied between full and 6% of full dose. A linear regression analysis of the data in Figure 4A gives a slope of $(3.55 \pm 0.10) \times 10^4$ s^{-1} which equals $k_{16obs}(2 \times 2.303)/(l\ \sigma_{RO2}(230\ nm))$; hence, $k_{16obs} = (5.4 \pm 0.7) \times 10^{-12}$ cm^3 molecule^{-1} s^{-1}.

In addition to reaction 16, the decay of the peroxy radical may also be influenced by reaction with CF_3O_2 radicals:

$$CF_3CH(O\bullet)OCH_2CF_3 + M \rightarrow CF_3CH_2OCHO + CF_3 \quad (20)$$

$$CF_3 + O_2 + M \rightarrow CF_3O_2 + M \quad (21)$$

$$CF_3CH(OO\bullet)OCH_2CF_3 + CF_3O_2 \rightarrow \text{products} \quad (22)$$

Since the rate constants for reactions 20−22 are unknown, we cannot correct for these reactions at the present time. Our reported value of k_{16obs} is the observed rate constant which describes the rate of decay of absorption at 230 nm in the present system. It is interesting to compare k_{16obs} with the rate constants for the self-reaction of other peroxy radicals. As discussed by Lesclaux,[12] the unsubstituted secondary peroxy radicals for which data are available (2-propyl, cyclopentyl, and cyclohexyl) undergo self-reaction with rate constants of the order of 10^{-15}−10^{-14} cm^3 molecule^{-1} s^{-1}. In contrast, the limited database for substituted secondary peroxy radicals ($CH_3CH(OH)CH(O_2)CH_3$, $CH_3CHBrCH(O_2)CH_3$, and $CF_3CH(O_2)CF_3$) suggests that such species are more reactive and undergo self-reaction with rate constants of the order of 10^{-13}−10^{-12} cm^3 molecule^{-1} s^{-1}. Our reported value of k_{16obs} provides further evidence of the high reactivity of substituted secondary peroxy radicals.

3.7. Rate Constant for the Reaction $CF_3CH(OO\bullet)OCH_2CF_3$ + NO → Products. Kinetic data were obtained by monitoring the increase in absorption at 400.5 nm ascribed to NO_2 formation following pulse radiolysis (dose = 22% of maximum) of mixtures of 10 mbar of $CF_3CH_2OCH_2CF_3$, 30 mbar of O_2, 960 mbar of SF_6, and 0.31−1.02 mbar of NO. Figure 6 shows typical experimental traces. For each NO concentration the increase in absorption was fitted using the CHEMSIMUL program[13] with the chemical mechanism in Table 2 and $\sigma(NO_2)_{400.5\ nm} = 6.5 \times 10^{-19}$ cm^2 molecule^{-1}.[14] The kinetic data in Table 2 were taken from the literature where available.[15−18] By analogy with other halogenated peroxy radicals[7,11] it was assumed that the formation of nitrate from reaction 3 is negligible. Two parameters, k_3 and k_{20}, were varied simultaneously to provide the fits to the experimental data shown in Figure 6. The fits were evaluated by visual inspection. The best fit values of k_3 were sensitive to the rate of increase in absorption while those for k_{20}, the decomposition rate of $CF_3CH_2OCHO(\bullet)CF_3$ radicals, were sensitive to the magnitude of the final absorption. For all transients the final absorption could be accounted for using $k_{20} = (7 \pm 2) \times 10^5$ s^{-1}. There are two competing loss mechanisms for $CF_3CH_2OCHO(\bullet)CF_3$ radicals in the reaction scheme in Table 2, and the value of k_{20} is actually determined relative to $k(CF_3CH_2OCHO(\bullet)CF_3 + NO)$ which is assumed equal to $k(CH_3O + NO)$. Accounting for uncertainties in $k(CF_3CH_2OCHO(\bullet)CF_3 + NO)$ we estimate that the value for k_{20} is accurate to within a factor of 2. The smooth curves in Figure 6A show the results of simulations using $k_3 = 1.45 \times 10^{-11}$ cm^3 molecule^{-1} s^{-1}, which gives acceptable fits of all the data. To illustrate the sensitivity to k_3, the dashed lines for the [NO] = 0.5 mbar data are simulations using $k_3 = 1.2$ and 1.7×10^{-11} cm^3 molecule^{-1} s^{-1}. We report a final value of $k_3 = (1.45 \pm 0.40) \times 10^{-11}$ cm^3 molecule^{-1} s^{-1}; the quoted uncertainty reflects the range of acceptable values of k_3 in the fits plus an additional 10% uncertainty because of the complex reaction mechanism used. This result is consistent with the kinetic data determined previously for reactions of other peroxy radicals with NO.[7,11]

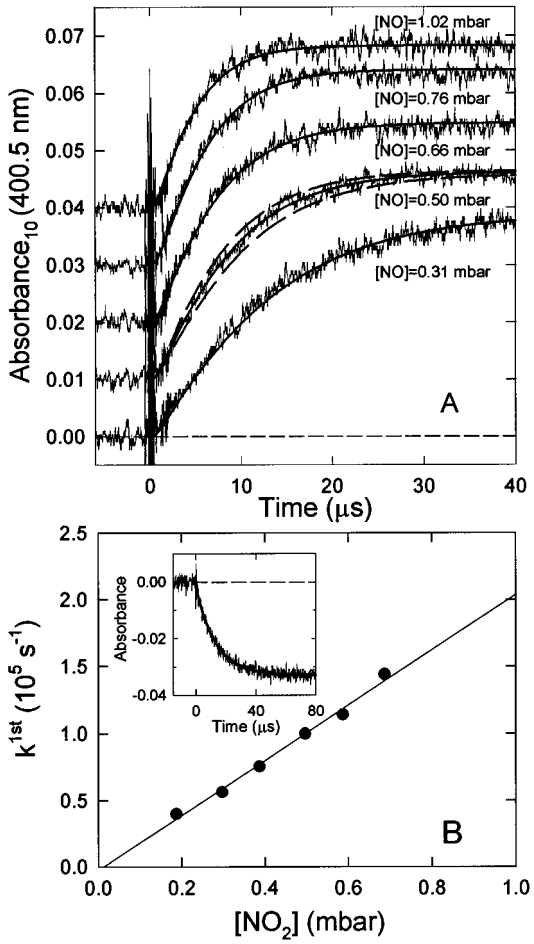

Figure 6. (A) Typical experimental traces following radiolysis of SF_6/$CF_3CH_2OCH_2CF_3$/O_2/NO mixtures, the smooth curves are fits to the data (see text for details). (B) Pseudo-first-order loss rates of NO_2 following radiolysis of SF_6/$CF_3CH_2OCH_2CF_3$/O_2/NO_2 mixtures versus the initial NO_2 concentration. The inset shows a typical experimental trace together with a first-order fit (see text for details).

TABLE 2: Reaction Mechanism Used to Fit the Experimental Data

reaction	rate constant (cm^3 molecule^{-1} s^{-1})	ref
F + RH* → R + HF[a]	1.5×10^{-11}	this work
F + NO + M → FNO + M	5.1×10^{-12}	15, 16
R + R + M → R_2 + M	2.6×10^{-11}	this work
R + O_2 + M → RO_2 + M	2.3×10^{-12}	this work
R + NO + M → RNO + M	1.5×10^{-11}	assumed
RO_2 + RO_2 → RO + RO + O_2	5.4×10^{-12}	this work
RO_2 + NO → RO + NO_2	1.4×10^{-11}	varied
RO_2 + NO_2 + M → RO_2NO_2 + M	8.4×10^{-12}	this work
RO + M → CF_3 + CF_3CH_2OCHO + M	7×10^5	varied
RO + NO + M → RONO + M	3.6×10^{-11}	*b*
CF_3 + O_2 + M → CF_3O_2 + M	4×10^{-12}	17
CF_3O_2 + NO → CF_3O + NO_2	1.6×10^{-11}	7, 11
CF_3O_2 + NO_2 + M → $CF_3O_2NO_2$ + M	7×10^{-12}	7, 11
CF_3 + NO + M → CF_3NO + M	1.6×10^{-11}	17

[a] R = $CF_3CH_2OCH(\bullet)CF_3$. [b] Assumed equal to $k(CH_3O + NO)$.[18]

3.8. Rate Constant for the Reaction $CF_3CH(OO\bullet)OCH_2CF_3 + NO_2 + M \rightarrow CF_3CH(OONO_2)OCH_2CF_3 + M$. Kinetic data were acquired by monitoring the decrease in absorption at 400.5 nm ascribed to NO_2 loss following pulse radiolysis (22% dose) of mixtures of 10 mbar of $CF_3CH_2OCH_2CF_3$, 30 mbar of O_2, 960 mbar of SF_6, and 0.19−0.69 mbar of NO_2. The inset in Figure 6B shows a typical experimental trace obtained using a mixture containing 0.39 mbar of NO_2. For each concentration of NO_2, the decrease in absorption was fitted using a first-order decay expression. The smooth line in the inset shows the result of such a fit. Figure 6B shows a plot of the resulting pseudo-first-order loss rates, k^{1st}, versus $[NO_2]$. Linear least-squares analysis of the data in Figure 6B gives $k_4 = (8.4 \pm 0.8) \times 10^{-12}$ cm^3 molecule^{-1} s^{-1}. The *y*-axis intercept is $-(3 \pm 9) \times 10^3$ s^{-1} and is not significant. The NO_2 loss can be calculated from the decrease in absorption using $\sigma(NO_2) = 6.5 \times 10^{-19}$ cm^2 molecule^{-1} [14] and when expressed in terms of the initial F atom concentration was 1.13 ± 0.19. The value of k_4 obtained here is similar to the high-pressure limiting rate constants for the reactions of other peroxy radicals with NO_2 which lie in the range $(5-10) \times 10^{-12}$ cm^3 molecule^{-1} s^{-1}.[7,11]

3.9. Relative Rate Studies of the Reactions of Cl Atoms with $CF_3CH_2OCH_2CF_3$ and $CF_3C(O)OCH_2CF_3$. Prior to investigating the products arising from the Cl atom initiated oxidation of $CF_3CH_2OCH_2CF_3$, relative rate experiments were performed using the FTIR setup to investigate the kinetics of the reaction of Cl atoms with $CF_3CH_2OCH_2CF_3$ and $CF_3C(O)OCH_2CF_3$. The relative rate technique is described in detail elsewhere.[19,20] Photolysis of molecular chlorine was used as a source of Cl atoms.

$$Cl_2 + h\nu \rightarrow 2Cl \quad (10)$$

The kinetics of reaction 11 were measured relative to those of reactions 23 and 24; reaction 25 was measured relative to reactions 26 and 27.

$$Cl + CF_3CH_2OCH_2CF_3 \rightarrow CF_3CH(\bullet)OCH_2CF_3 + HCl \quad (11)$$

$$Cl + CH_3Cl \rightarrow \text{products} \quad (23)$$

$$Cl + CH_3OCHO \rightarrow \text{products} \quad (24)$$

$$Cl + CF_3C(O)OCH_2CF_3 \rightarrow \text{products} \quad (25)$$

$$Cl + \text{HCFC-141b } (CH_3CCl_2F) \rightarrow \text{products} \quad (26)$$

$$Cl + CD_4 \rightarrow \text{products} \quad (27)$$

The observed loss of $CF_3CH_2OCH_2CF_3$ versus that of CH_3Cl and CH_3OCHO following the UV irradiation of $CF_3CH_2OCH_2CF_3/CH_3Cl/Cl_2$ and $CF_3CH_2OCH_2CF_3/CH_3OCHO/Cl_2$ mixtures in 700 Torr of total pressure of N_2 is shown in Figure 7A. Linear least-squares analysis gives $k_{11}/k_{23} = 1.43 \pm 0.07$ and $k_{11}/k_{24} = 0.52 \pm 0.03$. Using $k_{23} = 4.9 \times 10^{-13}$ [21] and $k_{24} = 1.4 \times 10^{-12}$ cm^3 molecule^{-1} s^{-1} [22] gives $k_{11} = (7.0 \pm 0.8) \times 10^{-13}$ and $(7.2 \pm 0.8) \times 10^{-13}$ cm^3 molecule^{-1} s^{-1}, respectively, where the quoted errors include a 10% uncertainty in the reference rate constants. We choose to quote a final value which is the average of the individual determinations with error limits that encompass the extremes of the individual determinations. Hence, $k_{11} = (7.1 \pm 0.9) \times 10^{-13}$ cm^3 molecule^{-1} s^{-1}.

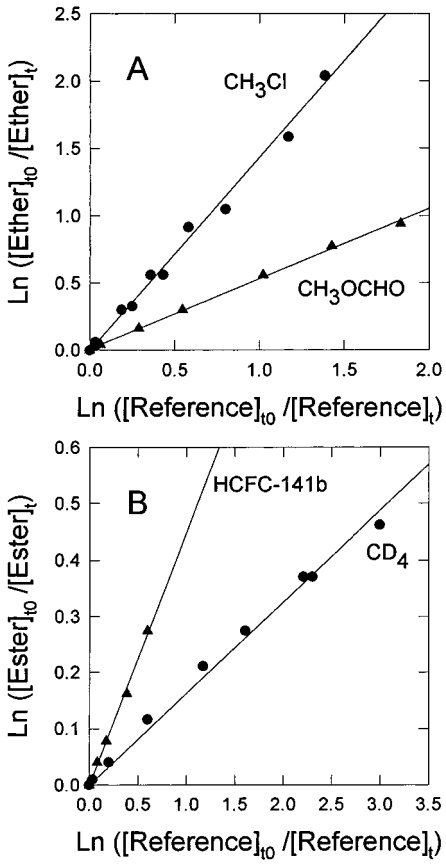

Figure 7. Plots of the decay of (A) $CF_3CH_2OCH_2CF_3$ (labeled "ether") versus CH_3Cl and CH_3OCHO and (B) $CF_3C(O)OCH_2CF_3$ (labeled "ester") versus HCFC-141b and CD_4 when mixtures containing these compounds were exposed to Cl atoms in 700 Torr of N_2. Solid lines are linear least-squares fits.

Figure 7B shows the observed decay of $CF_3C(O)OCH_2CF_3$, HCFC-141b, and CD_4 when mixtures of these compounds were exposed to Cl atoms in 700 Torr total pressure of N_2. From the data in Figure 7B, rate constant ratios of $k_{25}/k_{26} = 0.45 \pm 0.03$ and $k_{25}/k_{27} = 0.156 \pm 0.011$ are derived. Using $k_{26} = 2.0 \times 10^{-15}$ [20] and $k_{27} = 6.1 \times 10^{-15}$ [20] gives $k_{25} = (9.2 \pm 1.1) \times 10^{-16}$ and $(9.5 \pm 1.2) \times 10^{-16}$ cm^3 molecule^{-1} s^{-1}, respectively, where the quoted errors include a 10% uncertainty in the reference rate constants. We choose to quote a final value which is the average of the individual determinations with error limits that encompass the extremes of the individual determinations. Hence, $k_{25} = (9.4 \pm 1.3) \times 10^{-16}$ cm^3 molecule^{-1} s^{-1}. There are no literature data for k_{11} and k_{25} to compare with our results. It is, however, of interest to compare our value for k_{23} with the rate of reaction of Cl atoms with diethyl ether that proceeds with a rate constant of 3×10^{-10} cm^3 molecule^{-1} s^{-1} [23] which is at, or near, the gas kinetic limit. Making the reasonable assumption that abstraction of the H atoms from ethyl ether is statistical, it follows that reaction of Cl atoms with the $-CH_2-$ units in $CF_3CH_2OCH_2CF_3$ is a factor of 170 times slower than that in ethyl ether. Clearly, fluorine substitution has a dramatic effect on the reactivity the $-CH_2-$ groups (presumably by virtue of increasing the C−H bond strength).

3.10. Study of the Atmospheric Fate of $CF_3CHO(\bullet)OCH_2CF_3$ Radicals. To determine the atmospheric fate of the alkoxy radical $CF_3CHO(\bullet)OCH_2CF_3$ formed in reaction 3a, experiments were performed in which $CF_3CH_2OCH_2CF_3/NO/Cl_2/O_2$ mixtures at a total pressure of 700 Torr in N_2 diluent

were irradiated in the FTIR-smog chamber system:

$$CF_3CH(\bullet)OCH_2CF_3 + O_2 + M \rightarrow CF_3CH(OO\bullet)OCH_2CF_3 + M \quad (2)$$

$$CF_3CH(OO\bullet)OCH_2CF_3 + NO \rightarrow CF_3CH(O\bullet)OCH_2CF_3 + NO_2 \quad (3a)$$

$$CF_3CH(OO\bullet)OCH_2CF_3 + NO + M \rightarrow CF_3CH(ONO_2)OCH_2CF_3 + M \quad (3b)$$

The loss of $CF_3CH_2OCH_2CF_3$ and the formation of products were monitored by FTIR spectroscopy. There are three possible loss mechanisms for the alkoxy radical:

$$CF_3CH(O\bullet)OCH_2CF_3 + M \rightarrow CF_3CH_2OCHO + CF_3 + M \quad (20)$$

$$CF_3CH(O\bullet)OCH_2CF_3 + M \rightarrow CF_3C(O)H + CF_3CH_2O(\bullet) + M \quad (28)$$

$$CF_3CHO(\bullet)OCH_2CF_3 + O_2 \rightarrow CF_3C(O)OCH_2CF_3 + HO_2 \quad (29)$$

CF_3 radicals from reaction 20 will add O_2 and react with NO, leading to formation of COF_2:

$$CF_3 + O_2 + M \rightarrow CF_3O_2 + M \quad (21)$$

$$CF_3O_2 + NO \rightarrow CF_3O + NO_2 \quad (30)$$

$$CF_3O + NO \rightarrow COF_2 + FNO \quad (31)$$

If reaction 20 is the dominant fate of $CF_3CH(O\bullet)OCH_2CF_3$ radicals we expect to observe the formation of COF_2 and CF_3CH_2OCHO in molar yields of 100% (assuming that reaction 3b is of minor importance).

$CF_3CH_2O(\bullet)$ radicals from reaction 28 will react with O_2 to give $CF_3C(O)H$:[24]

$$CF_3CH_2O(\bullet) + O_2 \rightarrow CF_3C(O)H + HO_2 \quad (32)$$

The reactivity of $CF_3C(O)H$ toward Cl atoms is 2.5 times that of the ether $CF_3CH_2OCH_2CF_3$,[25] and it is expected that for the conversions of $CF_3CH_2OCH_2CF_3$ used in the present study (6−66%) secondary loss of $CF_3C(O)H$ via reaction 33 will be significant.

$$CF_3C(O)H + Cl \rightarrow CF_3CO + HCl \quad (33)$$

Under the present experimental conditions the CF_3CO radicals formed in reaction 33 will be converted into CF_3 radicals which, in turn, will be converted into COF_2 via reactions 21, 30, and 31:

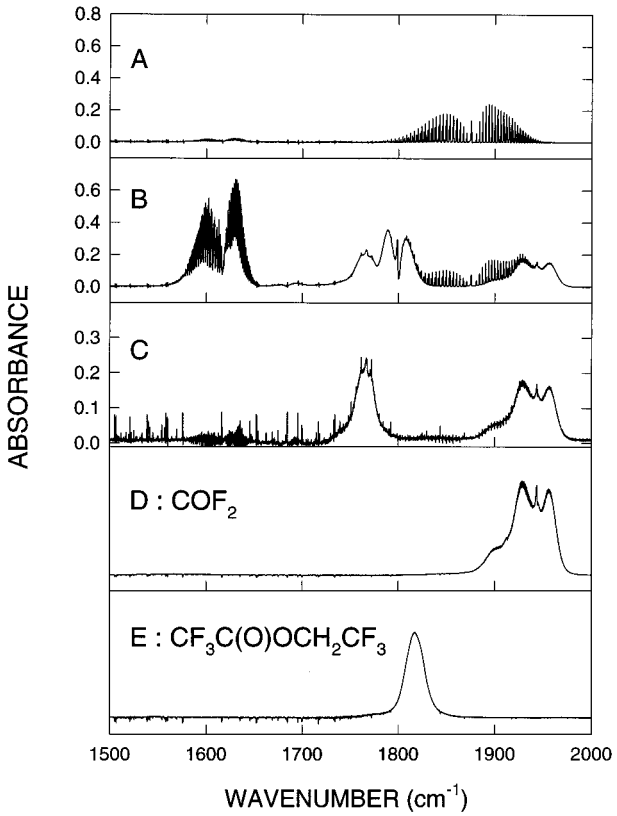

Figure 8. Spectra acquired before (A) and after (B) a 7 min irradiation of a mixture of 5.2 mTorr of $CF_3CH_2OCH_2CF_3$, 11 mTorr of NO, 174 mTorr of Cl_2, and 10 Torr O_2 in 700 Torr total pressure of N_2 diluent. Spectrum C was obtained by stripping features attributable to NO, NO_2, ClNO, and $ClNO_2$ from panel B. Panels D and E are reference spectra of COF_2 and $CF_3C(O)OCH_2CF_3$.

$$CF_3CO + O_2 \rightarrow CF_3C(O)O_2 \quad (34)$$

$$CF_3C(O)O_2 + NO \rightarrow CF_3CO(\bullet)O + NO_2 \quad (35)$$

$$CF_3CO(\bullet)O \rightarrow CF_3 + CO_2 \quad (36)$$

Thus, if reaction 28 is the dominant fate of $CF_3CHO(\bullet)OCH_2CF_3$ radicals we expect to observe the formation of COF_2 in a molar yield of 200%.

Four sets of experiments were performed with O_2 partial pressures of 10, 115, 400, and 600 Torr. Figure 8 shows spectra before (A) and after (B) irradiation of a mixture of 5.2 mTorr of $CF_3CH_2OCH_2CF_3$, 11 mTorr of NO, 174 mTorr of Cl_2, and 10 Torr of O_2 in 700 Torr total pressure with N_2. Spectrum C is obtained by stripping features attributable to NO, NO_2, ClNO, and $ClNO_2$ from panel B. Panels D and E are reference spectra of COF_2 and $CF_3C(O)OCH_2CF_3$. As seen from Figure 8C, while COF_2 was an observed product there was no observable formation of $CF_3C(O)OCH_2CF_3$ (<13% yield). The absence of $CF_3C(O)OCH_2CF_3$ suggests that reaction 29 is unimportant. Figure 9 shows a plot of the observed formation of COF_2 versus the loss of $CF_3CH_2OCH_2CF_3$. As seen in Figure 9, variation of the O_2 partial pressure by a factor of 60 had no discernible impact on the COF_2 yield, providing further support for the conclusion that reaction 29 is unimportant. Linear least-squares analysis of the data in Figure 9 gives a COF_2 yield of (90 ± 8)%. Quoted uncertainties are two standard deviations; in addition we estimate that possible systematic errors associated

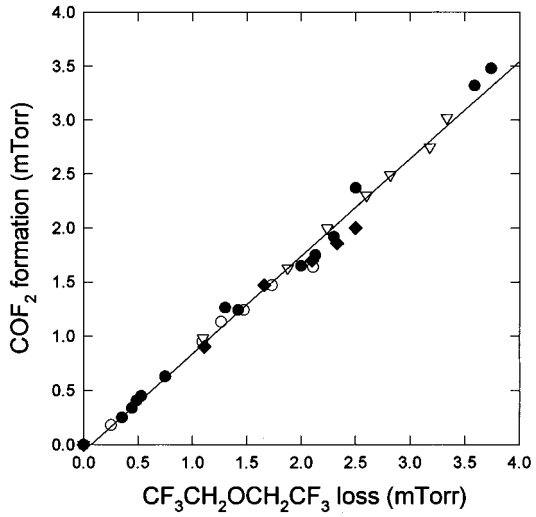

Figure 9. Plot of the observed yield of COF_2 versus the loss of $CF_3CH_2OCH_2CF_3$ following the irradiation of mixtures of 4.4−5.2 mTorr of $CF_3CH_2OCH_2CF_3$, 163−189 mTorr of Cl_2, 0−11 mTorr of NO, and 10 (▽), 115 (●), 400 (○), or 600 (◆) Torr of O_2 in 700 Torr total pressure of N_2 diluent at 295 K.

with calibration of the COF_2 and $CF_3CH_2OCH_2CF_3$ reference spectra contribute an additional 10% uncertainty range. Propagating this uncertainty leads to a final value for the COF_2 yield of 90 ± 12%.

The observation of a COF_2 yield of essentially 100% that is independent of the fractional loss of $CF_3CH_2OCH_2CF_3$ over the range 6−66% suggests that the sole atmospheric fate of $CF_3CH(O\bullet)OCH_2CF_3$ radicals is decomposition via elimination of a CF_3 group (reaction 20). Consistent with this conclusion a product feature at 1750−1800 cm^{-1} was observed in all experiments (see Figure 8C). This feature scaled linearly with the loss of $CF_3CH_2OCH_2CF_3$ and has a frequency consistent with that expected for the carbonyl stretching mode of the formate $CF_3CH_2OC(O)H$. From the linear increase of CF_3CH_2OCHO we conclude that $k_{37} < 0.5 \times k_{11}$, hence $k_{37} < 4 \times 10^{-13}$ cm^3 $molecule^{-1}$ s^{-1}.

$$Cl + CF_3CH_2OCHO \rightarrow \text{products} \qquad (37)$$

The simulated atmospheric oxidation of $CF_3CH_2OCH_2CF_3$ in the presence of NO has also been studied by O'Sullivan et al.[26] Consistent with the results from the present work, O'Sullivan et al.[26] report the formation of $CF_3CH_2OC(O)H$ and COF_2 as major products with a yield of ≫90% in air. O'Sullivan et al.[26] also report the formation of $CF_3C(O)OCH_2CF_3$ and that the yield of this product increased in experiments conducted in O_2. In contrast to the results of O'Sullivan et al.,[26] in the presence of NO we did not observe any formation of $CF_3C(O)OCH_2CF_3$ (yield < 13%) even in the presence of 600 Torr of O_2. From the upper limit for the $CF_3C(O)OCH_2CF_3$ yield measured here we can derive an upper limit for the rate constant ratio $k_{29}/k_{20} < 8 \times 10^{-21}$ cm^3 $molecule^{-1}$. At 295 K in 1 atm of air < 4% of $CF_3CH(O)\cdot OCH_2CF_3$ radicals undergo reaction with O_2.

For completeness, a limited series of experiments was performed using $CF_3CH_2OCH_2CF_3/Cl_2/O_2/N_2$ reaction mixtures (as above but without NO). Interestingly, a small (ca. 15%) yield of the ester $CF_3C(O)OCH_2CF_3$ was observed. However the yield of the ester was unaffected by variation of the O_2 partial pressure over the range 10−700 Torr and we conclude that the ester is formed in reaction 16b, or 5b, or both, and not via reaction 29.

$$2\ CF_3CH(OO\bullet)OCH_2CF_3 \rightarrow 2\ CF_3CH(O\bullet)OCH_2CF_3 + O_2 \qquad (16a)$$

$$2\ CF_3CH(OO\bullet)OCH_2CF_3 \rightarrow CF_3C(O)OCH_2CF_3 + CF_3CH(OH)OCH_2CF_3 + O_2 \qquad (16b)$$

$$CF_3CH(OO\bullet)OCH_2CF_3 + HO_2 \rightarrow CF_3CH(OOH)OCH_2CF_3 + O_2 \qquad (5a)$$

$$CF_3CH(OO\bullet)OCH_2CF_3 + HO_2 \rightarrow CF_3C(O)OCH_2CF_3 + H_2O + O_2 \qquad (5b)$$

Implications for Atmospheric Chemistry. We present herein a large body of kinetic and mechanistic data pertaining to the atmospheric chemistry of bis(2,2,2-trifluoroethyl) ether. The atmospheric lifetime of bis(2,2,2-trifluoroethyl) ether is determined by its reaction with OH radicals and has been estimated to be ≫114 days.[26] Reaction with OH gives the alkyl radical $CF_3CH(\bullet)OCH_2CF_3$. In 1 atm of air this alkyl radical has a lifetime of 84 ns with respect to addition of O_2 to give the corresponding peroxy radical $CF_3CH(OO\bullet)OCH_2CF_3$. We show here that the peroxy radical reacts rapidly with NO to produce NO_2 and, by inference, $CF_3CH(O\bullet)OCH_2CF_3$ radicals. Using $k_3 = 1.4 \times 10^{-11}$ cm^3 $molecule^{-1}$ s^{-1} together with an estimated background tropospheric NO concentration of 2.5×10^8 molecule cm^{-3}, the lifetime of the peroxy radicals with respect to reaction with NO is calculated to be 5 min. Reaction 3 is likely to be an important atmospheric loss of $CF_3CH(OO\bullet)OCH_2CF_3$ radicals. The sole fate of the alkoxy radical derived from bis(2,2,2-trifluoroethyl) ether is decomposition via C−C bond scission to give 2,2,2-trifluoroethyl formate (CF_3CH_2OCHO) and a CF_3 radical. This behavior is entirely consistent with the available database concerning the behavior of similar nonfluorinated alkoxy radicals, e.g., $C_2H_5OCH(O\bullet)CH_3$ and $(CH_3)_3COCH(O\bullet)CH_3$ radicals are known to decompose via C−C bond scission to give formates.[27] It is reported herein that the formate CF_3CH_2OCHO is rather unreactive toward Cl atoms and is likely to be similarly unreactive toward OH radicals. Organic compounds which react with Cl atoms with rate constants in the range 10^{-14}−10^{-13} cm^3 $molecule^{-1}$ s^{-1} generally react faster with Cl atoms than with OH radicals. Hence, we can use the value of $k_{37} < 4 \times 10^{-13}$ cm^3 $molecule^{-1}$ s^{-1} as an upper limit to $k(OH + CF_3CH_2OCHO)$. Using the structure−reactivity relationship approach[28] gives an estimate of the reactivity of the $-CH_2-$ group in CF_3CH_2OCHO toward OH attack of 1.1×10^{-13} cm^3 $molecule^{-1}$ s^{-1}. In typical formates (methyl formate, ethyl formate etc.) the formate group itself is considered to make a negligible contribution to the overall reactivity of the molecule, and consequently structure−reactivity factors for the formate group are not available. In the case of CF_3CH_2OCHO the reactivity of the formate group may make a significant contribution to the overall reactivity and it is difficult to estimate the overall reactivity of CF_3CH_2OCHO toward OH radicals. Using a 24 h global average OH concentration of 1×10^6 cm^{-3} and $k(OH + CF_3CH_2OCHO) < 4 \times 10^{-13}$ cm^3 $molecule^{-1}$ s^{-1}, we derive a lower limit of 30 days for the atmospheric lifetime of CF_3CH_2OCHO with respect to reaction with OH radicals. In view of the polar nature of CF_3CH_2OCHO it seems likely that the main atmospheric removal mechanism of this compound will be via wet/dry

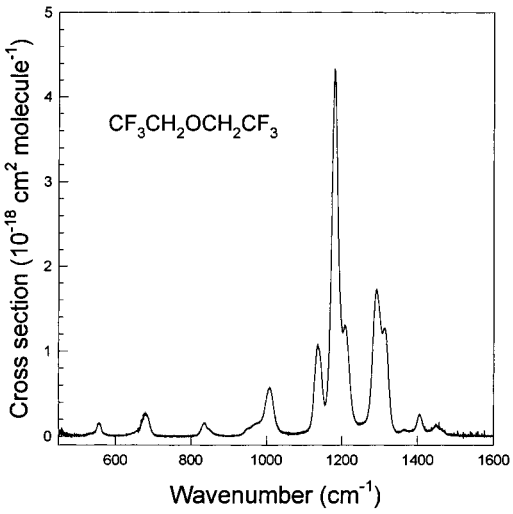

Figure 10. IR spectrum of $CF_3CH_2OCH_2CF_3$.

deposition and possibly photolysis. There are no available data for the rates of these processes and hence it is not possible to provide an estimate of the atmospheric lifetime of CF_3CH_2-OCHO at this time.

The atmospheric degradation of HFEs produce the same fluorinated radical species as formed during the degradation of HFCs. HFCs do not impact stratospheric ozone[3] and the same conclusion applies to HFEs. Bis(2,2,2-trifluoroethyl) ether has an ozone depletion potential of zero. Finally we need to consider the potential for bis(2,2,2-trifluoroethyl) ether to impact the radiative balance in the atmosphere. Using the method of Pinnock et al.[29] with the IR spectrum shown in Figure 10 we calculate instantaneous forcings for bis(2,2,2-trifluoroethyl) ether and CFC-11 of 0.35 W/m^2 and 0.26 W/m^2, respectively. Values of the GWP (global warming potential) for bis(2,2,2-trifluoroethyl) ether (relative to CFC-11) can then be estimated using the expression

$$\mathrm{GWP}_{\mathrm{ether}} = \left(\frac{\mathrm{IF}_{\mathrm{ether}}}{\mathrm{IF}_{\mathrm{CFC-11}}}\right)\left(\frac{\tau_{\mathrm{ether}} M_{\mathrm{CFC-11}}}{\tau_{\mathrm{CFC-11}} M_{\mathrm{ether}}}\right)\left(\frac{1-\exp(-t/\tau_{\mathrm{ether}})}{1-\exp(-t/\tau_{\mathrm{CFC-11}})}\right)$$

where IF_{ether}, IF_{CFC-11}, M_{ether}, M_{CFC-11}, t_{ether}, and t_{CFC-11} are the instantaneous forcings, molecular weights, and atmospheric lifetimes of the two species and t is the time horizon over which the forcing is integrated. Using $t_{ether} \gg 114$ days[26] and $t_{CFC-11} = 50$ years,[29] we estimate that the GWP of bis(2,2,2-trifluoroethyl) ether is $\gg 0.019$ for a 20 year horizon and $\gg 0.007$ for a 100 year time horizon. The GWP of bis(2,2,2-trifluoroethyl) ether is modest.

Acknowledgment. The work at Risø was supported by the European Union. We thank Mike Hurley (Ford) for providing Figure 10, Steve Japar (Ford) for helpful comments, and Roger Atkinson (University of California) for advice on SAR calculations.

References and Notes

(1) Molina, M. J.; Rowland, F. S. *Nature* **1974**, *249*, 810.

(2) Farman, J. D.; Gardiner, B. G.; Shanklin, J. D. *Nature* **1985**, *315*, 207.

(3) Wallington, T. J.; Schneider, W. F.; Worsnop, D. R.; Nielsen, O. J.; Sehested J.; Debruyn, W. J.; Shorter, J. A. *Environ. Sci. Technol.* **1994**, *28* (8), 320.

(4) Sehested, J. Ph.D. Thesis, 1994.

(5) Hansen, K. B.; Wilbrandt, R., Pagsberg, P. *Rev. Sci. Instr.* **1979**, *50*, 1532.

(6) Wallington, T. J.; Japar, S. M. *J. Atmos. Chem.* **1989**, *9*, 399.

(7) Wallington, T. J.; Dagaut, P.; Kurylo, M. J. *Chem. Rev.* **1992**, *92*, 667.

(8) Wallington, T. J.; Ellermann, T.; Nielsen, O. J. *Res. Chem. Intermed.* **1994**, *20*, 265.

(9) Wallington, T. J.; Hurley, M. D.; Maricq, M. M.; Sehested, J.; Nielsen, O. J.; Ellermann, T. *Int. J. Chem. Kinet.* **1993**, *25*, 651.

(10) Ellermann, T.; Sehested, J.; Nielsen, O. J.; Pagsberg, P.; Wallington T. J. *Chem. Phys. Lett.* **1994**, *218*, 287.

(11) Lightfoot, P. D.; Cox, R. A.; Crowley, J. N.; Destriau, M.; Hayman, G. D.; Jenkin, M. E.; Moortgat, G. K.; Zabel, F. *Atmos. Environ.* **1992**, *26A*, 1805.

(12) Lesclaux, R. Combination of peroxyl radicals in the gas phase. In *Peroxyl radicals*; Alfassi, Z., Ed.; John Wiley: New York, 1997.

(13) Rasmussen, O. L., Bjergbakke, E. B., Lynggaard, B., Pagsberg, P.; Kirkegaard, P. *CHEMSIMUL*. Risoe National Laboratory: Roskilde, Denmark, (9306), 1993. 1993.

(14) Sehested, J.; Christensen, L. K.; Møgelberg, T. E.; Nielsen, O. J.; Wallington, T. J.; Guschin, A.; Orlando, J. J.; Tyndall, G. S. *J. Phys. Chem. A*, in press.

(15) Sehested, J.; Ellermann, T.; Nielsen, O. J.; Wallington, T. J. *Int. J. Chem. Kinet.* **1994**, *26*, 615.

(16) Wallington, T. J.; Ellermann, T.; Nielsen, O. J.; Sehested, J. *J. Phys. Chem.* **1994**, *98*, 2346.

(17) Kaiser, E. W.; Wallington, T. J.; Hurley, M. D. *Int. J. Chem. Kinet.* **1995**, *27*, 205.

(18) Atkinson, R.; Baulch, D. L.; Cox, R. A.; Hampson, R. F.; Kerr, J. A.; Rossi, M. J.; Troe, J. *J. Phys. Chem. Ref. Data* **1997**, *26*, 521.

(19) Wallington, T. J.; Hurley, M. D.; Shi, J.; Maricq, M. M.; Sehested, J.; Nielsen, O. J.; Ellermann, T. *Int. J. Chem. Kinet.* **1993**, *25*, 651.

(20) Wallington, T. J.; Hurley, M. D. *Chem. Phys. Lett.* **1992**, *189*, 437.

(21) DeMore, W. B.; Sander, S. P.; Golden, D. M.; Hampson, R. F.; Kurylo, M. J.; Howard, C. J.; Ravishankara, A. R.; Kolb, C. E.; Molina, M. J. Jet Propulsion Laboratory Publication 94-26, Pasadena, CA, 1994.

(22) Wallington, T. J.; Hurley, M. D.; Ball J. C.; Jenkin M. E. *Chem. Phys. Lett.* **1993**, *211*, 41.

(23) Mallard, W. G.; Westley, F.; Heron, J. T.; Hampson, R. F. *NIST Chemical Kinetics Database, Version 6.0*, 1994.

(24) Nielsen, O. J.; Gamborg, E.; Sehested, J.; Wallington, T. J.; Hurley, M. D. *J. Phys. Chem.* **1994**, *98*, 9518.

(25) Wallington, T. J.; Hurley, M. D. *Int. J. Chem. Kinet.* **1993**, *25*, 819.

(26) O'Sullivan, N.; Wenger, J.; Sidebottom, H. W. The oxidizing capacity of the troposphere. *Proceedings of the Seventh European Commission symposium on physicochemical behavior of atmospheric pollutants*, Venice, Italy, October 1996; Larsen, B., Versino, B., Eds.; p 77.

(27) Japar, S. M.; Wallington, T. J.; Richert, J. F. O.; Ball. J. C. *Int. J. Chem. Kinet.* **1990**, *22*, 1257.

(28) Kwok, E. S. C.; Atkinson, R. *Atmos. Environ.* **1995**, *29*, 1685.

(29) Pinnock, S.; Hurley, M. D.; Shine, K. P.; Wallington, T. J.; Smyth, T. J. *J. Geophys. Res.* **1995**, *100*, 23227.